A Simple Approach for Boundary Improvement of Euler Diagrams

Category: Research

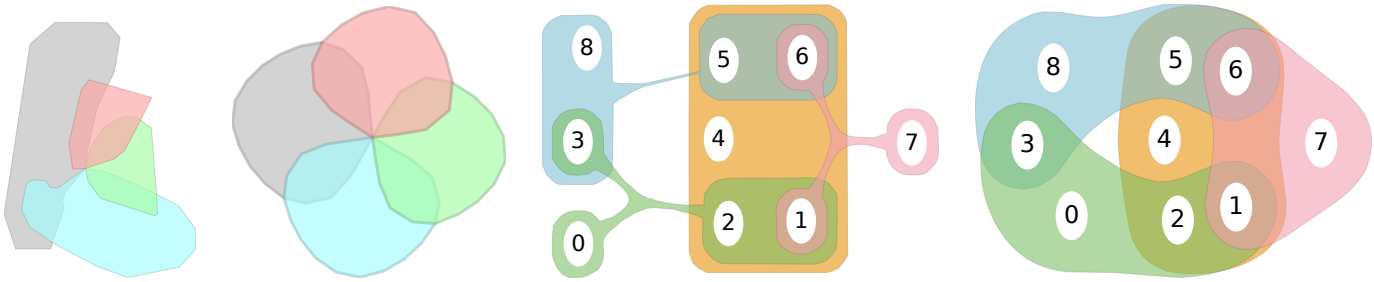

(a) (b) (c) (d)

Fig. 1: Boundary smoothing for existing Euler diagrams. (a) General Euler diagram [18, Fig. 6b] reproduced. (b) The result of the improvement (c) An Untangled diagram [17, Fig. 5b] reproduced. (d) The result of the improvement.

Abstract— Euler diagram drawing methods that are able to produce a drawing for every input instance of sets and their intersections require irregular polygons. Yet, empirical evidence indicates that rounder contours perform better when reading these diagrams. In this paper, we present a simple method that can be applied to the output of any Euler diagram drawing approach to improve the smoothness of the diagram boundaries. When refining the input diagram, we must ensure that set elements remain inside their appropriate boundaries and that areas of the diagram do not appear/disappear. Our approach uses a force system that ensures that the topological structure of the input diagram does not change during refinement while improving the diagram. We demonstrate the effectiveness of our approach through case studies and metric evaluations.

Index Terms—Euler diagrams, Boundary Improvement, Force-Directed Approaches

1 Introduction

Euler diagrams [10] are an intuitive way to visualize sets and their contents, because they visualize set content in the most straightforward way possible: sets in these diagrams are polygons and if the polygons overlap, the sets intersect. Recent techniques aim at automating the process of drawing Euler diagrams with closed curves to directly visualize the intersections of sets. Elements membership can easily be represented using enclosure by these curves. Given a list of sets and their intersections, these general techniques are powerful enough to produce a drawing for any input instance [18, 21, 8, 17, 20, 3]. Because these drawing are intuitive, Euler diagrams have been an important visualization technique applied in various fields including: bioinformatics [4, 11], digital humanities [28], social networks [15], multimedia database queries [27], and many others.

An issue with these general techniques is the shape of the polygons that represent the sets in these drawings are often jagged and elongated due to the large number of constraints that the drawing must satisfy to be valid. Intuitively, rounder polygons are more aesthetically pleasing. Empirical evidence provides support for smooth closed curves as they pop out visually [12, 26, 16], and early empirical evidence into the readability of Euler diagrams suggests that smooth set contours are perceptually more effective [6]. Thus, an approach that is able to transform the output of any of the above approaches into a smoother diagram has the potential to improve its aesthetics and its readability.

In this paper, we introduce a simple method that is able to significantly improve the boundaries of any Euler diagram drawing approach that uses polygons and their overlap to indicate the relationship between sets of elements. The approach proposed is a highly simplified form of *curve shortening flow* for shape improvement [24, 25, 9, 31, 7] applied to the problem of Euler diagram drawing. Such techniques, which have often been used in geometry processing, graphics, and scientific visualization, to our knowledge, have not been applied to the problem of Euler diagram drawing or the area of information visualization in general. The essence of our approach is to derive a new force system based on boundary curvature. This force system can be applied in conjunction with diagram constraints to greatly improve the appearance of the Euler diagram while ensuring a correct drawing.

The primary contribution of this paper is an algorithm that combines a simplified form of curve shortening flow with Euler diagram drawing methods to improve the smoothness of any Euler diagram drawn with curves. The approach we propose is general and can be applied to the output of all Euler diagram drawing methods that represent sets as closed curves and intersections as overlap between those curves. Our approach is significantly more scalable than existing techniques to improve the smoothness of Euler diagrams. More importantly, the approach can guarantee a valid drawing for every input instance. Thus, the refined drawing has precisely the same topology as the Euler diagram provided as input – at no point are intersections between the polygons created or destroyed during refinement. Finally, the approach is easy to implement, consisting of only four forces, greatly simplifying the algorithm when compared to competitive approaches. We demonstrate the effectiveness of this method through case studies and metric evaluations that compare our proposed technique to state-of-the-art techniques.

2 Related work

The related work for this work combines two seemingly disparate areas of work: shape improvement and Euler diagram drawing. In this section, we describe the related work in these areas and how they can be combined to improve the curvature of Euler diagrams.

2.1 Shape Improvement and Mean Curvature Flow

Mean curvature flow is a classic method for smoothing shapes. Each point on the curve (in two dimensions) or the surface (in three dimensions) is moved in the direction of the normal in a way that is proportional to its curvature. This process *flattens* the object [9]. Unfortunately, mean curvature flow also also tends to *shrink* the object,

which may not be desired.

Taubin [24, 25] proposes λ-μ smoothing which is a classic method to avoid shrinking of the surface during smoothing. The approach works by alternating the direction of improvement at every other step. Taubin shows that his proposed algorithm, λ-μ smoothing, is able to smooth out rough parts of the model while preserving volume through an elegant analogy to Fourier space operations – the algorithm essentially reduces the amount of energy in high-frequency components while preserving the total amount of energy in the system. In this paper, we use the principle behind λ-μ to move vertexes of the boundary along the direction of curvature. However, as set elements are located inside the diagram, we can use the repulsive forces of the elements for area preservation.

2.2 Euler Diagram Drawing

Methods for visualizing sets and their intersections has been an active area of research in recent years with many novel visualization approaches developed for this purpose [3]. As the algorithm we propose in this work improves diagrams that represent sets as polygons, we focus on these methods for set visualization in this section. However, it is important to note that other approaches exist for visualizing sets and their intersections that are based on circles [11, 22, 29], ellipses [13], and approaches that are not based on closed curves at all [1, 2].

A number of approaches are able to produce a drawing for every input instance. Rodgers *et al.* introduce a method for drawing a subclass of Euler diagrams [19], and then extend this research to work on any input instance [18]. In these approaches, the dual graph of the Euler diagram is transformed into a planar graph for drawing. Then, a triangulation is used to route set contours through the plane, creating a diagram. Simonetto *et al.* [21] propose a force-directed solution that is guaranteed to produce a correct drawing. In this approach, a planar representation of the Euler diagram is computed and drawn initially with a planar graph drawing algorithm. Subsequently, the drawing is improved using a modification of the `PrEd` [5] graph drawing algorithm to ensure that the structure of the Euler diagram does not change, nodes and edges do not cross boundaries during force-directed refinement, and that elements of the sets stay in their proper zones. This approach was further improved in later work [20], allowing for boundaries with adaptive complexities and faster convergence. Collins *et al.* [8] describe a method for drawing Euler diagrams when the elements of the sets have fixed positions. The approach relies on marching squares and implicit curves to derive the boundaries for each set. Riche and Dwyer [17] describe a method where splits to the sets involved in the diagram are connected with edges and an approach that prioritizes containment. Stapleton *et al.* [23] present a method for inductively adding curves to a diagram and preserving well-formedness properties in the drawing.

The research proposed is a simple approach for improving the appearance of any Euler diagrams drawn using polygons. In fact, we demonstrate our technique operating on the output of many of these algorithms [21, 8, 17, 14].

The closest work to our own is `EulerForce` [14] where boundaries and curve positions have been modified to improve the readability of the Euler diagram. This approach is based on a force system, consisting of fourteen forces, to optimize the shape of the curves in the diagram, driving them towards circular shapes.

In contrast, the approach presented in this paper is fundamentally different than this approach. Our force system is simpler, consisting of only four forces, which helps improve complexity in terms of execution speed and implementation. The results are more scalable and able to refine Euler diagrams of realistic complexity beyond the five or so sets of `EulerForce`. Finally, and most importantly, our approach can be configured to never produce an invalid drawing — that is, we can impose constraints such that no new zones are created or destroyed by the refinement procedure.

3 Method

In this section, we present a description of the proposed approach. Firstly, we describe how our simplified version of curve shortening flow can be adapted in order to optimize the smoothness of polygons. Then, we will analyse differences and similarities between the original and the adapted formulation of this method. Finally, we identify additional requirements needed in order to successfully apply this method to the optimisation of Euler diagrams.

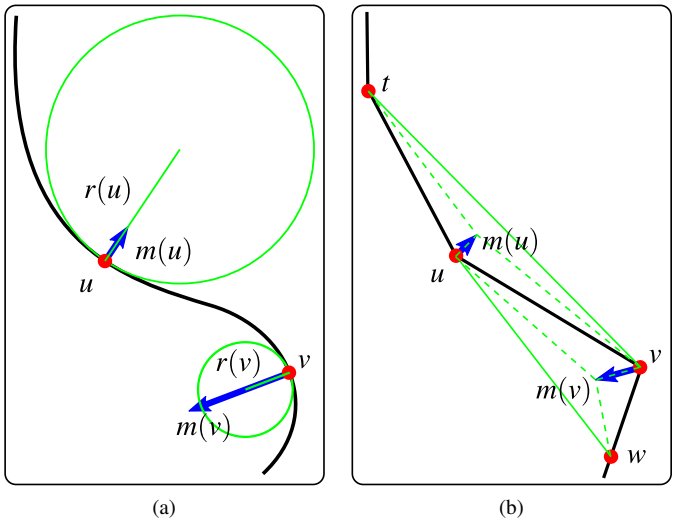

(a) (b)

Fig. 2: Curve Shortening Flow. (a) In the original formulation of the problem, each point of the curve moves towards the centre of its osculating circle with speed proportional to the curvature at that point. (b) We adapt this problem to polylines by moving each point u of a boundary to the centroid of the triangle $\triangle tuv$, where t and v are the neighbour bends of u.

3.1 Discrete Curve Shortening Flow

Curve shortening flow is defined on a continuous curve and continuous time, ideally requiring the computation of infinite points for infinitesimal increments of time (see Fig. 2a). Instead, the optimization of Euler diagrams operates in discrete time and space, as vertex positions can only be optimized on a discrete basis and the curves themselves are modelled as polylines. Thus, we must adapt the original method to:

- *Discrete Space.* The concept of curvature, which is well defined for a sufficiently smooth curve, cannot be directly applied to a vertex u of a polygon $\ldots tuv\ldots$. The centre of curvature should be placed perpendicular to the line normal at u, but this line is not uniquely defined as the slope of the secant for a left and right increment from u only correspond when t, u, v are collinear.
- *Discrete Time.* In continuous curve shortening flow, the movement speed of a point can approach infinity when the radius of the osculating circle approaches zero. In continuous time this never occurs, as the speed of the vertex is re-calculated after an infinitesimally small period of time in the new lower stress position of the vertex. However, in discrete time, the time period t cannot be infinitesimally small, and therefore points with high speed will cause abrupt movements in t. Put simply, we require a more conservative approach to node movement in order to reduce the impact of large movements.

When defining our method for computing direction and intensity of movement, the properties of the original formulation must be preserved as much as possible. This formulation should be easy to implement and fast to compute. A solution that adequately satisfies all of these requirements computes the movement of a vertex u in $\ldots tuv\ldots$ along the vector that connects u to the centroid of the triangle $\triangle tuv$ (see Fig. 2b).

Definition 1. Given a polygon $p = p_0 \ldots p_n$, we define *smoothing on* p_i as the operation that transforms p into $p' = p_0 p_{i-1} b p_{i+1} \ldots p_n$ where b is the centroid of $\triangle p_{i-1} p_i p_{i+1}$.

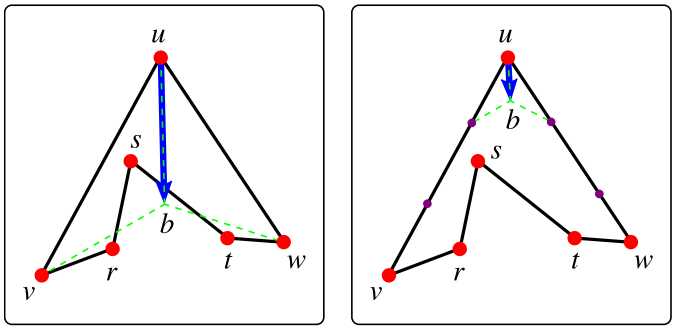

Fig. 3: Smoothing a concave polygon. (a) The smoothing operation of a vertex u would cause a self-intersection. (b) The chance of creating a self intersection is reduced by re-sampling the polygon to obtain smaller edges with uniform length. By adding the new bends (purple circles), the previous smoothing operation has no self intersections.

Definition 2. Given a polygon $p = p_0 \dots p_n$, we define *smoothing on* p as the application of smoothing on each polygon vertex p_i.

3.2 Comparison with Curve Shortening Flow

We describe properties of the centroid smoothing technique defined above and we discuss similarities and differences between the definitions of discrete and continuous curve shortening flow.

Theorem 1. *Given a convex polygon p, by performing smoothing on any of its vertexes, we obtain a polygon p' that is still convex.*

Proof. A polygon is convex iff all its internal angles are equal or less than 180°. Let $p = \dots tuv \dots$ and u be the vertex selected for smoothing. Since p is convex, the internal angles of t, u and v are equal or less than 180°. By performing smoothing on u, we substitute u with the centroid b of $\triangle tuv$. This operation does not increase the internal angle of vertexes t and v, which will still be equal or less than 180°. Also, since the centroid of $\triangle tuv$ is contained in $\triangle tuv$, the angle $\angle tbv$ is not greater than 180°. Since all other internal angles remain unchanged, all the internal angles of the polygon are not greater than 180°, which means p' is still convex. □

Lemma 1. *Given a convex polygon p, by performing smoothing on any of its vertexes, we obtain a polygon p' whose boundary do not self-intersect.*

Proof. As p is convex, p' is also convex and therefore simple. □

Theorem 2. *Each polygon p asymptotically converges to a single point by repeatedly applying smoothing on p.*

Proof. Let us consider a vertex u of a polygon $\dots tuv \dots$. If u is not collinear with t and v, by moving u to the centroid b of $\triangle tuv$, the polygon edge tu becomes tb and the polygon edge uv becomes bv, both of which are shorter than the original edges (or $\overline{tu} + \overline{uv} > \overline{tb} + \overline{bv}$). If u collinear with t and v, the edges computed after smoothing u will have a total length equal to the original edges ($\overline{tu} + \overline{uv} = \overline{tb} + \overline{bv}$). Since not all polygon vertexes p_i can be collinear with the line defined by p_{i-1} and p_{i+1}, repeated application of smoothing on the polygon results in a sequence of polygons $p, p', p'' \dots$ of strictly decreasing perimeter. Since the polygon edges have positive lengths, the perimeter tends to zero or exactly the same point. □

The previous theorems show that the discrete curve shortening preserves non-crossing properties for convex polygons, and that the asymptotic results of the two flows correspond for any polygon. However, the first property does not hold for concave polygons, as shown in Fig. 3a.

By re-sampling the polygon borders the chance of self intersection is reduced, as shown in Fig. 3b. Our experiments verify that this procedure is sufficient for avoiding self-intersections. However, if avoiding self-intersections is strictly required, we can enable used in previous work [5, 20] reduce movement to a safe distance whenever this movement can cause self intersections.

Border re-sampling however provides a second, crucial advantage. When a polygons are over-sampled, refinement of the boundaries is impeded. In fact, a vertex u is very close to neighbours t and v, the triangle $\triangle tuv$ is small and therefore its centroid is close to u. Therefore, the re-sampling can reduce curve complexity, improving the speed of the computation.

3.3 Preservation of Diagram Properties

Discrete curve shortening flow provides a method for curve simplification. However, it cannot be used directly for Euler diagrams improvement without first ensuring that it will preserve fundamental diagram properties such as the presence or absence of set intersections and element containment. First, boundaries should not shrink to a point. As Euler contain set elements in the interior of the curves, we use these elements as a backstop, allowing set boundaries to nicely shrink to fit the elements they contain and preventing the diagram from collapsing to a point. In section 4, we discuss this in further detail.

Secondly, sufficient spacing between set elements as well as between set elements and set boundaries needs to be ensured. Therefore, we propose to model discrete curve shortening flow using a force-directed algorithm, allowing us to use other forces to ensure proper spacing.

Finally, we must prevent set elements from crossing boundaries and ensure that set intersections in the diagram are neither created nor destroyed. This property is accomplished by constraining node movement.

4 Implementation

In this section, we describe the implementation of a force-directed algorithm that can be used to improve the appearance of Euler diagrams through discrete curve shortening flow. First, we explain how the input diagram, the output of any Euler diagram drawing method, is encoded into a graph. Then, we present the algorithm itself, `EulerSmooth`. Finally, we discuss how the algorithm can be configured and its parameters to improve the diagrams presented in this paper.

4.1 Input Diagram

The input diagrams are modelled as graphs with polyline edges. These graphs have two sets of nodes: the set elements and the boundary junctions. The set elements have degree zero and have position, colour, size and labels. The junctions identify crossing points between boundaries of the original diagram. These nodes are connected with polyline edges that follow the boundary contours with arbitrary precision. Sets with no boundary crossings are still identified with a singular junction, that is placed in a random point of the set boundary, closing a polyline loop (see Figs. 4a and 4b). For each set, we identify a subgraph formed by all the elements contained in that set, and all junctions and edges that compose its boundary (see Fig. 4c).

This construction ensures that any crossings and concurrent boundaries are modified simultaneously over all sets, preserving the original topology of the graph. We define this condition as *dependent boundaries*. Whenever this behaviour is considered too restrictive, is it possible relax these constraints and duplicate junctions and shared edges so that the duplicated elements share the same initial position but are free to evolve separately. We define this configuration as *independent boundaries* (see Fig. 4d). In this paper, all the input diagrams have been constructed by manually tracing over output images, constructing this graph.

4.2 `EulerSmooth`

The proposed algorithm can be considered a modular version a force-directed approach. In the implementation (see Algorithm 1), forces, constraints, and post-iterations steps are modules that can be plugged into or removed from the algorithm, providing a flexible approach.

The input corresponds to the Euler diagram represented as a graph composed of polyline edges. Polyline bends and segments are treated

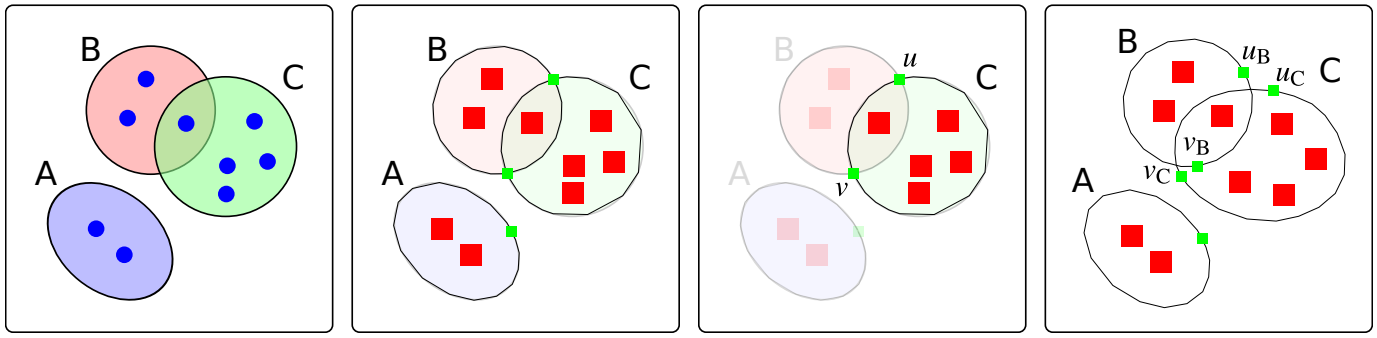

(a) (b) (c) (d)

Fig. 4: The input diagram. (a) The original diagram the algorithm aims to improve. (b) The diagram is modelled as a graph. In green, the junctions. Polyline edges define the set boundaries. (c) For each set, we identify a subgraph containing all graph elements contained by that set. This subfigure shows the subgraph for set C. (d) We can choose to use independent boundaries, allowing for a less constrained refinement. Junctions and edges shared between subgraphs are duplicated (*e.g.* u is duplicated in u_B and u_C), allowing for separate refinement.

Algorithm 1 `EulerSmooth`.

for numberOfIterations **do**

  for all $v \in V$ **do**
    force$(v) \leftarrow 0$
    constraint$(v) \leftarrow +\infty$

  ▷ FORCE COMPUTATION
  for all ForceDef in ForceSystem **do**
    force $\leftarrow$ force + ForceDef.compute()

  ▷ CONSTRAINT COMPUTATION
  for all ConstraintDef in ConstraintSystem **do**
    constraint $\leftarrow$ min (constraint, ConstraintDef.compute())

  ▷ NODE MOVEMENT
  for all $v \in V$ **do**
    if magnitude(force(u)) $>$ constraint(u) **then**
      force$(u) \leftarrow$ force$(u) *$ constraint$/$magnitude(force(u))
    position$(u) \leftarrow$ position(u) + force(u)

  ▷ POST-ITERATION
  for all PostIteration in PostIterationSteps **do**
    PostIteration.compute()

by most modules as if they were standard nodes and edges. However, we support polyline edges to differentiate elements of the drawing that can be added/removed (polyline bends and segments) versus those that must remain in the drawing (nodes and whole edges). All modules use a QuadTree data structure to accelerate the computation time.

In the following, we will discuss the modules these modules, starting with the forces, then the constraints, and finally the post processing steps.

4.2.1 Forces

`EulerSmooth` allows flexibility in defining the force system to be used. In particular, for all forces it is possible to indicate subsets of the graph elements to which the force is applied. Also, the technique can load multiple instances of the same force, allowing it, for example, to enforce different distances between elements in the drawing according to their role.

In the following, we indicate with $\boldsymbol{p}_u \in \mathbb{R}^2$ the position of the node u. If $e = (u,v)$ is an edge, we indicate the line segment delimited by $\boldsymbol{p}_u$ and $\boldsymbol{p}_v$ as $\boldsymbol{p}_e$.

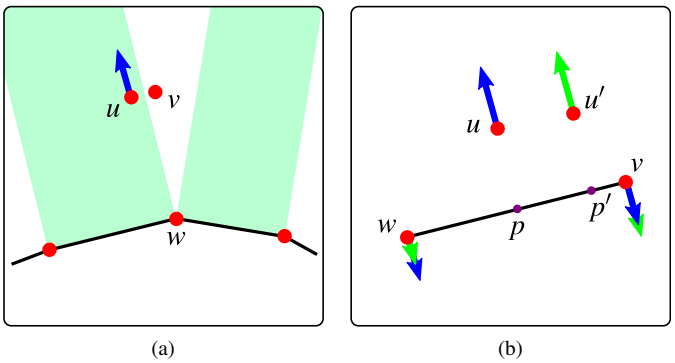

(a) (b)

Fig. 5: Edge repulsion force modifications. (a) The related `ImPrEd` force is null if the node projection is not contained in the edge. As a result, a node might alternate between being affected or not by edge repulsion even with the slightest modification of position. The problem is solved by incorporating a repulsion force between the node and the closest edge extremity when the node projection is not contained in the edge. (b) The forces exerted on the edge extremities depend on their distance to p, providing a balancing effect on the forces.

EdgeAttraction(d) This force attracts the extremities of an edge toward each other, decreasing the length of the edge. The parameter d indicates the ideal distance under which the force starts becoming weak. The attractive force $\mathscr{F}_u^a$ acting on the node u of the edge $e = (u,v)$ is:

$$\mathscr{F}_u^a(e,d) = \left(\frac{\|\boldsymbol{p}_u - \boldsymbol{p}_v\|}{d}\right)(\boldsymbol{p}_v - \boldsymbol{p}_u)$$

NodeNodeRepulsion(d) This force repels two nodes from each other. The parameter d indicates the ideal distance under which the force intensifies. As is usual for force-directed algorithms, the attraction and repulsion balance close to d. The repulsive force $\mathscr{F}_u^r$ is defined as:

$$\mathscr{F}_u^r(u,v,d) = \left(\frac{d}{\|\boldsymbol{p}_u - \boldsymbol{p}_v\|}\right)^2(\boldsymbol{p}_u - \boldsymbol{p}_v)$$

EdgeNodeRepulsion(d) This force repels nodes from nearby edges. The parameter d as a similar meaning than for the force above. This force has been modified from its original formulation in `ImPrEd` to improve the force stability of node-boundary configurations (Fig. 5).

Let u be a node, $e = (v,w)$ be an non-incident edge ($u \notin e$). Let p be the projection of u on the line defined by e. We define v as the closest edge extremity to u. The repulsive force $\mathscr{F}_u^e$ is:

$$\mathscr{F}_u^e(u,e,d) = \begin{cases} \left(\frac{d}{\|\boldsymbol{p}_u - \boldsymbol{p}_p\|}\right)^2 (\boldsymbol{p}_u - \boldsymbol{p}_p) & \text{if } p \in \boldsymbol{p}_e \\ \mathscr{F}_u^r(u,v,d) & \text{otherwise} \end{cases}$$

The respective forces on the segment extremities are:

$$\mathscr{F}_v^e(u,e,d) = \begin{cases} -\mathscr{F}_u^e(u,e,d)\frac{\|\boldsymbol{p}_p - \boldsymbol{p}_w\|}{\|\boldsymbol{p}_v - \boldsymbol{p}_w\|} & \text{if } p \in \boldsymbol{p}_e \\ -\mathscr{F}_u^r(u,v,d) & \text{if } p \notin \boldsymbol{p}_e \end{cases}$$

$$\mathscr{F}_w^e(u,e,d) = \begin{cases} -\mathscr{F}_u^e(u,e,d)\frac{\|\boldsymbol{p}_p - \boldsymbol{p}_v\|}{\|\boldsymbol{p}_v - \boldsymbol{p}_w\|} & \text{if } p \in \boldsymbol{p}_e \\ \mathbf{0} & \text{if } p \notin \boldsymbol{p}_e \end{cases}$$

The factor introduced in the first cases intensify the repulsive force on the closest edge extremity and decreases it on the farther one, better approximating the behaviour of an analogue physical system (see Fig. 5b).

CurveSmoothing This force implements the smoothing effect of the discrete curve shortening flow. The force moves a node toward the centroid of the triangle formed with its neighbours. Therefore, the $\mathscr{F}_u^s$ acts on node u with neighbours t and v is:

$$\mathscr{F}_u^s = \frac{2}{3}\left(\frac{\boldsymbol{p}_t + \boldsymbol{p}_v}{2} - \boldsymbol{p}_u\right)$$

4.2.2 Constraints

These modules can be used to control node movements or avoid movements that could compromise the properties of the drawing that we want to preserve. In this section, we describe these constraints.

DecreasingMaxMovement(d) This constraint sets a maximal movement for all nodes which starts at a value of d and linearly decreases to 0 as the computation progresses, allowing for a precise final positioning.

MovementAcceleration(d) This constraint influences movement consistency in the algorithm. For each node v, a constraint $c_i(u)$ is updated according to the angle a between consecutive iterations:

$$c_i(u) = \begin{cases} d & \text{if } i = 0 \\ c_{i-1}(1 + 2(1 - \frac{a}{60^\circ})) & \text{if } a < 60^\circ \\ c_{i-1} & \text{if } 60 \leq a < 90^\circ \\ c_{i-1}/(1 + 4(\frac{a}{90^\circ} - 1)) & \text{if } a \geq 90^\circ \end{cases}$$

In other words, the constraint is multiplied by a factor in the range $[1,3]$ for movement in the same direction and divided by $[1,5]$ for movement in opposite directions. This greatly reduces node oscillation.

PinnedNodes This module that set to 0 the movement constraint of a given set of nodes, forcing them to keep their original position.

SurroundingEdges Given a set nodes V and a set of edges E, the module ensures no $u \in V$ can cross any edge $e \in E$. For a given u and $e = (v,w)$, the module identifies a line l that divides the plane into two halves. If the projection p of u in e lies in the edge ($p \in \boldsymbol{p}_e$), the line l is identified as the axis of symmetry of the segment up. If the projection lies outside the edge, l is the axis of symmetry of the segment uv, with v being the closest endpoint to u. This module ensures that u and e by limiting their movement to the collision distance between node and l along the direction of movement (see Fig. 6).

4.2.3 Post-Iteration Steps

Post-iteration modules allow for the processing of the output of each iteration.

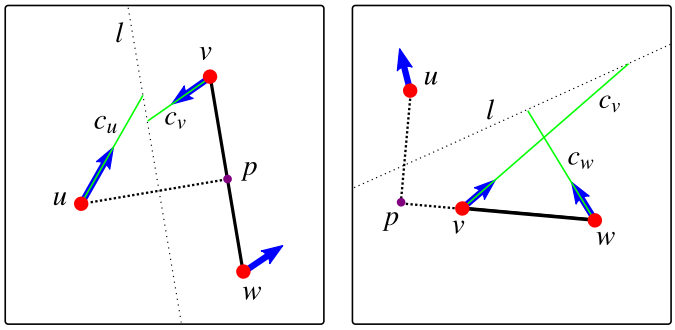

(a) (b)

Fig. 6: Surrounding edge constraint. The module defines a line l that separates a node and and edge that should not be crossed. We ensure crossings will not occur by restricting the nodes movements to be smaller than the collision distance between c_x with l. When the force does not point towards l, no constraint is necessary. (a) Constraint computation for p when it lies on the edge. (b) Constraint computation for p when it lies outside the edge.

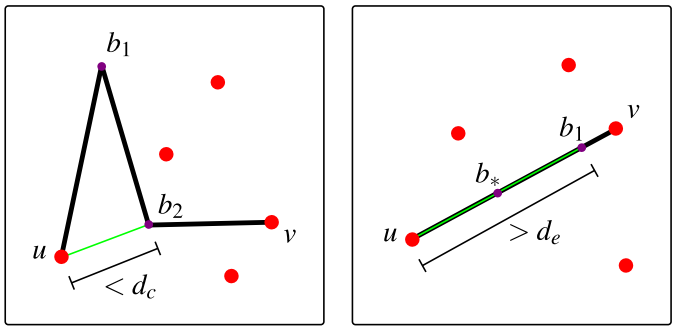

(a) (b)

Fig. 7: Flexible edges contraction and expansion. (a) Contraction. Since b_1 previous bend (u) and following bend (b_2) are closer than d_c and no nodes are in the triangle $\triangle ub_1b_2$, the bend b_1 and its incident segments are substituted by the green segment. (b) Expansion. Since the first edge segment is longer than d_e, a new bend b_* is introduced and the segment is substituted by the two green ones.

FlexibleEdges(d_c, d_e) Provides the flexible edge functionality of `ImPrEd`. Given an edge set E, the module increases or decreases the number of bends depending on the stress of its edge segments. Given an edge e, the module first tries to contract the edge, by removing bends, and then it tries to expand it by adding them. When contracting an edge, the module marks $b_1 \ldots b_n$ for removal. The bend b_i is removed if the distance between its previous bend b_{i-1} (edge source, if $i = 1$) and the next bend b_{i+1} (edge target, if $i = n$) is less than d_c and no node is contained in the triangle formed by the three bends (see Fig. 7a). When expanding an edge, the segments $e_1 \ldots e_n$ are checked for expansion. A segment is expanded when its length is greater than d_e by inserting a new bend at its midpoint (see Fig. 7b).

4.3 Algorithm Configuration

Despite its modular nature, configuring `EulerSmooth` is simple. In order to ensure comparable results, we run the same algorithm configuration for all the diagrams in this paper. This requires a single distance parameter d^* and setting three boolean variables. The parameter d^* can be thought of as an ideal distance between set elements and between set elements and boundaries. This parameter is proportional to the scale of the imported diagram.

The core modules, loaded for the improvement of each diagram, are:

CurveSmoothing
EdgeNodeRepulsion(d^*) between elements and boundary edges
EdgeAttraction(0.7 d^*) for boundary edges
DecreasingMaxMovement(d^*)
MovementAcceleration(d^*)
FlexibleEdges(1.45 d^*, 1.5 d^*)

The curve smoothing module drives the boundary improvement and all other modules are defined as above.

The first boolean indicates if dependent or independent set boundaries are required (see Section 4.1). We denote `Dep` to indicate dependant boundaries and `Ind` to indicate independent boundaries:

if `Dep` **then**
    SurroundingEdges between all nodes and boundaries.
else
    SurroundingEdges between elements and boundaries.

Through surrounding edges, we prevent set elements and boundaries from crossing and ensure that set elements do not leave the set. As this behaviour can be turned on or off for boundary nodes, when off it will allow for the creation or elimination of new zones that are not in the original diagram. The general result is a smoother diagram, where some new empty zones can be created. However if this behaviour is not desired and the precise topology of the diagram needs to be preserved, surrounding edges can be applied to all nodes in the drawing, including boundary nodes, ensuring that no new zone is created or destroyed by the procedure.

The second boolean option pins element movement. We use `Fix` to indicate fixed position and `Mov` to indicate free moving elements:

if `Fix` **then**
    PinnedNodes on set elements
else
    NodeNodeRepulsion(d^*) between set elements

Pinning elements is particularly useful when refining drawings such as those produced by Bubble Sets [8]. Otherwise, forces are applied to set elements in order to optimize their distribution.

The final boolean allows concurrency between set boundaries to be turned on and off. We use `Sep` to indicate the activation of this option:

if `Sep` **then**
    EdgeNodeRepulsion(d^* / 15) between boundary nodes and edges

When set, a small radius repulsive force between nodes and unrelated boundary edges is inserted, creating a separation between collinear boundaries. This option improves the readability of diagram, but could generate unnecessary stress and boundary irregularity on diagrams without concurrent boundaries.

For all images presented in this paper, we specify the options set to generate them.

5 Analysis

To evaluate the effectiveness of `EulerSmooth`, we extracted diagrams published in previous work and tried to improve them. The initial diagrams have been created by tracing contours and adding set elements as prescribed by the output images. Then, these diagrams have been optimized using appropriate parameters for a given case. For example, when improving the Manhattan Bubble Sets diagram (see Figure 13), we use fixed node positions as they are prescribed by the locations on the map. Whenever applicable, we improved the diagram using options, to showcase the many outputs available with `EulerSmooth`.

Contour Based Diagrams Euler diagrams drawing approaches might or might not show set elements, causing significant differences in how a diagram is created and interpreted. For example, in a diagram that does not represent set elements (contour based), the existence of a overlap in the diagram implies that the given intersection contains elements. On the other hand, requirement is not strict for element based approaches, since elements present in the region determine if it is empty or not.

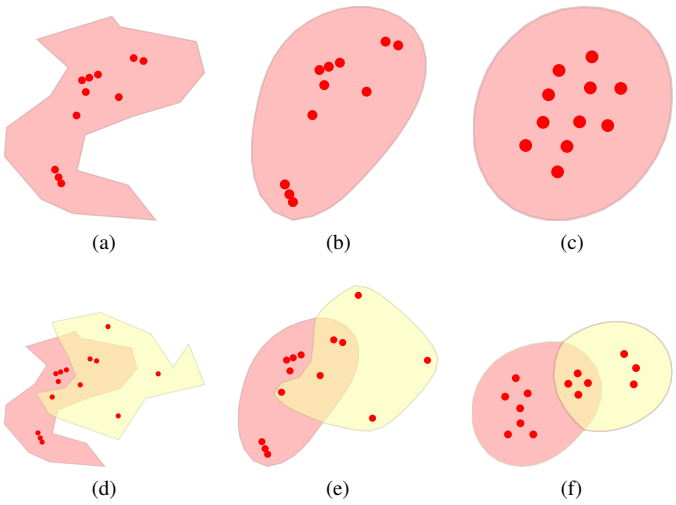

Fig. 8: Example diagrams optimised with `EulerSmooth`. (a,d) The original diagrams. (b,e) The diagrams optimised while keeping the nodes in their original position (`Fix`,`Dep`). (c,f) The diagrams optimised while allowing elements move (`Mov`,`Dep`).

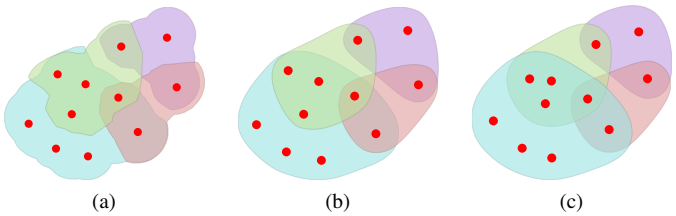

Fig. 9: Optimization of a `Set Visualiser` diagram [30]. (a) The original diagram reconstructed. (b) The diagram optimised while keeping the nodes in their original position (`Fix`,`Ind`). (c) The diagram optimised while allowing elements move (`Mov`,`Ind`).

For this reason, the two approaches are not always directly comparable. In our case, since the algorithm assumes the diagram is element based and requires set elements to limit shrinking, we need to adapt contour based approaches by adding a dummy element to each region. We do this for the diagrams in Figure 12.

Testing Hardware and Software All images and results in this section are generated by a Java implementation of `EulerSmooth`, which include a testing GUI that shows the progress of the diagram smoothing, computes diagram statistics, and record the running times. The source code of the application and executable library (jar) are available: **(hidden for double blind review, jar included in submission)**.

All computation have been performed on a desktop machine equipped with an Intel Core i7-2600 processor, 8GB of RAM, and running KDE 4.14 on Arch Linux.

5.1 Qualitative Evaluation

Figure 8 shows the results of `EulerSmooth` on two basic diagrams: one with a single set and a second with two overlapping sets. We notice how the contour regularity is improved both when enabling or disabling element movement, but `EulerSmooth` achieves a better result when the nodes can be moved into more desirable positions.

Figure 9 shows an improved version of a diagram generated with `Set Visualiser` [30]. By using independent boundaries, we can eliminate an unnecessary empty zones (blue-only region in the top-centre) which might make the original diagram less readable. We notice little difference between the results obtained with fixed versus

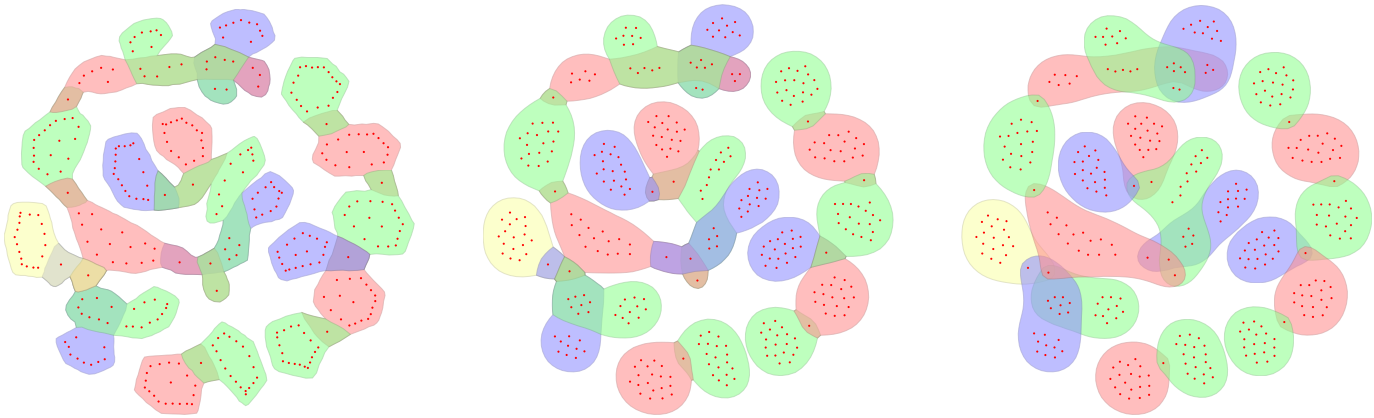

(a) (b) (c)

Fig. 10: Optimization of the Imdb20 Euler diagram [21, Figure 9a]. (a) The original reconstructed. (b) The diagram optimised while allowing elements to move (`Mov`,`Dep`). (f) The diagram optimised allowing elements move and sets evolve independently (`Mov`,`Ind`).

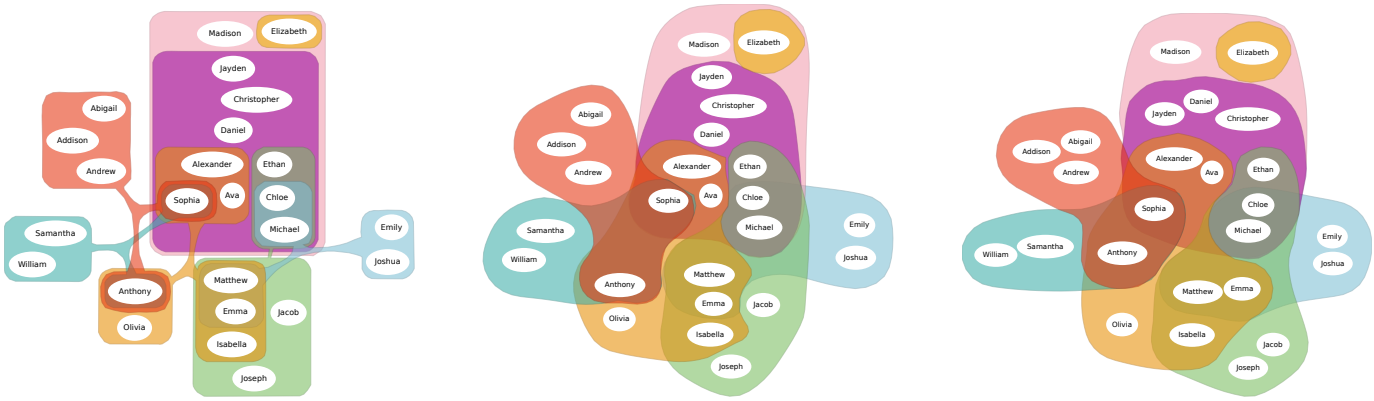

(a) (b) (c)

Fig. 11: Optimization of an Untangled Euler diagram [17, Figure 1a]. (a) The original diagram reconstructed. (b) The diagram optimised while keeping the nodes in their original position (`Fix`,`Ind`). (c) The diagram optimised while allowing elements to move (`Mov`,`Ind`).

movable elements as the initial positions of set elements do not require much adjustment.

Figure 10 shows the optimization of a diagram from Euler Representation [21, Figure 9a] consisting of 20 sets. This figure illustrates the difference between dependent and independent boundaries. In the first case, all regions of the original diagrams are preserved throughout the smoothing process, meaning that no new zones are created or undone. This forces concurrent boundaries to be maintained, limiting improvement. In particular, examine the blue set at the top of Figure 10b: on the right side the set crosses two other boundaries (green and red) at a single point. Since that point must assume a position that must satisfy three different curves, we obtain unpleasant sharp angles for two boundaries (blue and green).

If preserving the exact topology of the initial diagram is less of a priority, we enable independent boundaries and obtain the results in Figure 10c. By enabling this option, we introduce new regions not present in the original drawing (in Figure 10c, see for instance blue-only triangular region in the centre of the drawing). However, none of these new regions will contain elements and the boundaries are much easier to trace.

Figure 12 shows the same input diagram improved with `EulerSmooth` and `EulerForce`. The diagrams improved with `EulerForce` look more regular as quantitative analysis can confirm. However, the shapes obtained with `EulerSmooth` are smooth and readable.

Figure 13 shows application of our method to the Manhattan Bubble Sets [8, Figure 9]. Although the obtained sets are far from circles, `EulerSmooth` can simplify boundaries even in these constrained circumstances, improving the ability to trace these contours.

Finally, in Figure 11, `EulerSmooth` is applied to an Untangled Euler diagram [17, Figure 1a], transforming it into a more classical looking one (whenever this is desired) with regular boundaries.

5.2 Quantitative Evaluation

We evaluated the effectiveness of `EulerSmooth` in smoothing the set boundaries by computing the average initial and final isoperimetric quotient for the diagram sets. Given a closed curve ℓ, the isoperimetric quotient computes the ratio between the area enclosed by the line and that of a circle with equal circumference: $Q = 4\pi \text{ area}(\ell) \,/\, \text{length}(\ell)$.

Since circles are the shape that maximize closed area for a given perimeter, all simple closed curves will have an isoperimetric quotient between 0 and 1. This value is computed for each set in the diagram and averaged.

Improvements over Various Techniques Table 1 reports options used, running time, and initial and final average isoperimetric quotient for the diagrams in this paper. We notice that our approach improves Q over all cases with larger improvements when less restrictive options are enabled (`Mov` instead of `Fix`, `Ind` instead of `Dep`). A low smoothing value is obtained for Bubble Sets (Figure 13), which is a heavily constrained diagram that is difficult to improve.

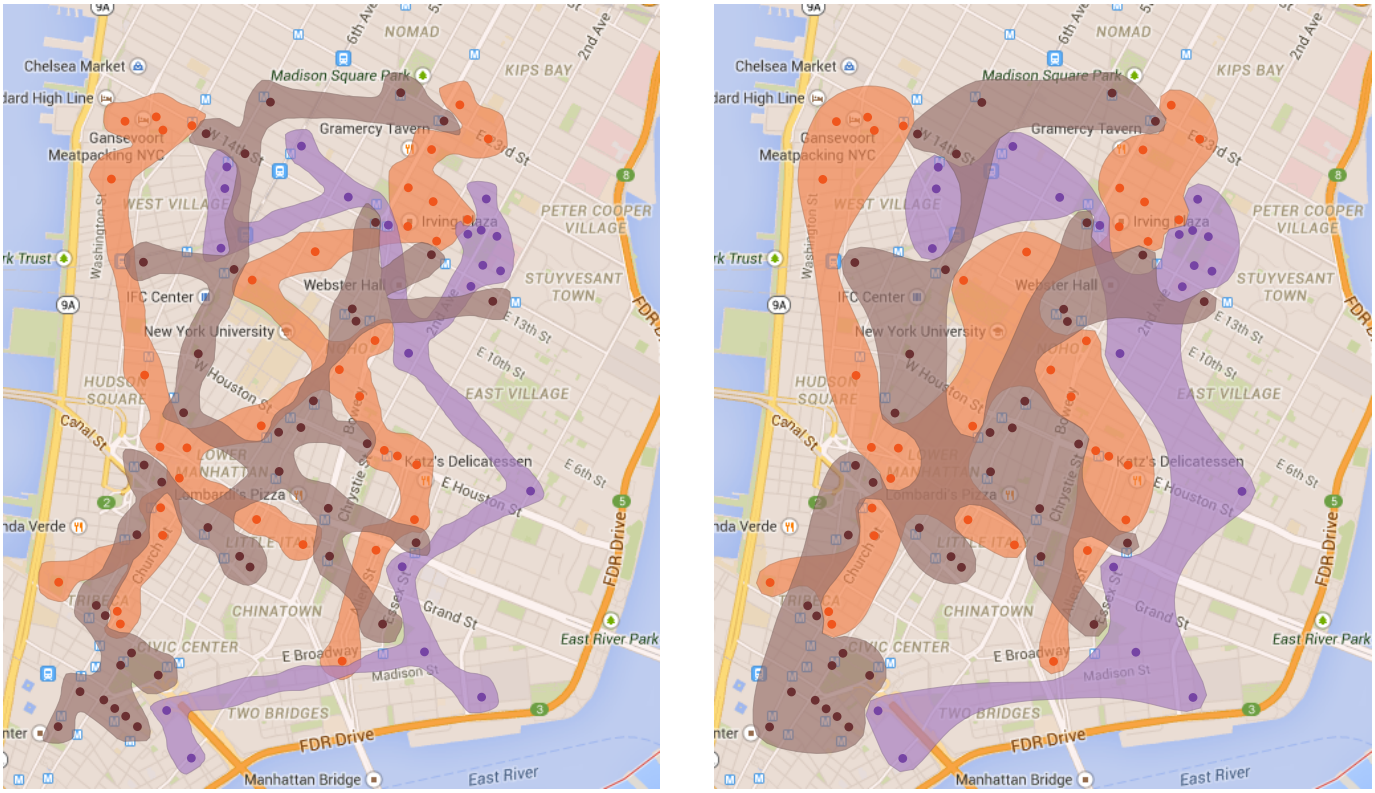

(a) (b)

Fig. 13: Improvement of Bubble Sets diagram over the Manhattan map [8, Figure 9]. (a) The original diagram reconstructed. (b) The diagram optimised with `EulerSmooth` (`Fix`,`Ind`).

Diagram	Fig.	Opt.	Iter.	Q_i %	Q_s %	Time (s)
General Euler	1b	MD	300	75.3	96.5	3.35
Untangled Small	1d	MI	100	36.7	76.3	2.42
Single	8b	FD	120	39.7	90.3	1.83
	8c	MD			99.6	1.96
Double	8e	FD	120	45.7	85.3	1.88
	8f	MD			98.5	2.07
Imdb20	—	FD	25	56.9	74.6	6.52
	—	FI	40		84.6	9.67
	10b	MD	25		73.9	6.71
	10c	MI	40		86.0	10.15
BubbleSet	13b	FI	50	4.5	10.2	6.43
Untangled	11b	FI	100	47.1	79.2	5.25
	11c	MI			82.8	5.21
SetVis	9b	FI	50	77.3	92.3	1.22
	9c	MI			93.3	1.19

Table 1: Statistics for the execution of `EulerSmooth` over the diagrams in this paper. The statistics for EulerForce diagrams (Figures 12 and 14) are collected in Table 2. Constraints activated are indicated by their first letter (F for `Fix`, M for `Mov`, D for `Dep`, I for `Ind`). Iterations shows the number of smoothing cycles performed. Q_i is the initial average isoperimetric quotient. Q_s is the average isoperimetric quotient for the improved diagram. The running time is the average running time over five runs of the approach.

Sets	Id	Q_i %	Q_s %	Q_f %	Time$_s$ (s)	Time$_f$ (s)
3	1	58.3	95.5	99.0	3.6	2.35
	2	57.0	95.6	98.5	3.5	3.48
	3	51.3	96.1	98.6	3.6	2.25
	4	51.0	96.2	97.4	4.6	2.57
	5	58.5	95.5	98.8	5.9	2.57
4	1	53.6	96.2	98.1	5.4	4.85
	2	38.4	93.9	94.0	5.7	5.85
	3	45.5	94.9	97.2	6.2	4.63
	4	41.9	93.3	93.0	4.5	6.14
	5	53.6	95.6	98.5	5.1	5.85
5	1	36.5	84.9	Inv	8.6	32.89
	2	41.7	95.2	98.2	8.2	16.64
	3	43.0	95.6	95.0	8.2	14.53
	4	44.3	86.2	Inv	13.9	25.67
	5	42.6	85.6	Inv	13.5	22.47

Table 2: Statistics for the improvement of diagrams with `EulerSmooth` and `EulerForce`. Q_x is the average isoperimetric quotient. Subscript i indicates initial, s indicates `EulerSmooth`, f indicates `EulerForce`. Q_f has not been computed for the three 5-sets instances (ID 1, 4 and 5) as `EulerForce` produced invalid diagrams. On all diagrams, we run `EulerSmooth` with the option `Mov`, `Dep` and `Sep`. For 3 and 4 sets, 350 iterations were sufficient. For 5 sets, we ran 500 iterations.

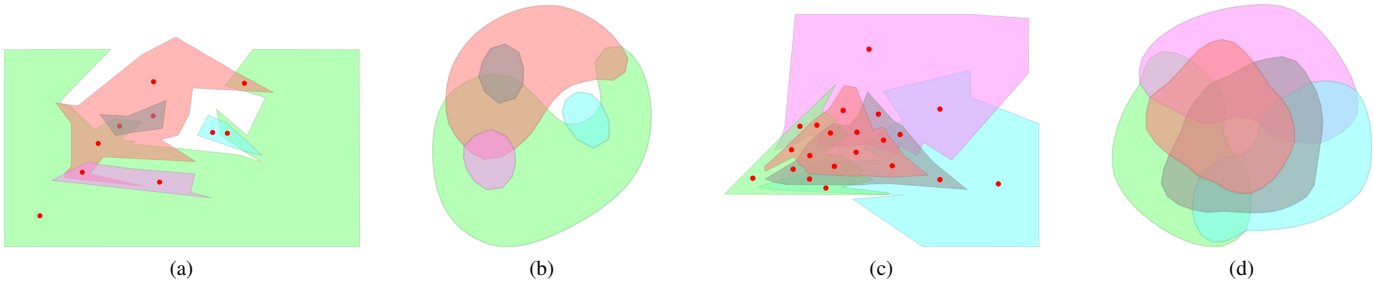

Fig. 14: Optimization of two five-set diagrams unsupported by `EulerForce`. (a,c) The initial diagram (reconstructed from the `EulerForce` software). (b,d) The diagrams optimised with `EulerSmooth` (`Mov`,`Dep`,`Sep`). The dummy elements have been removed to re-create a contour based diagram.

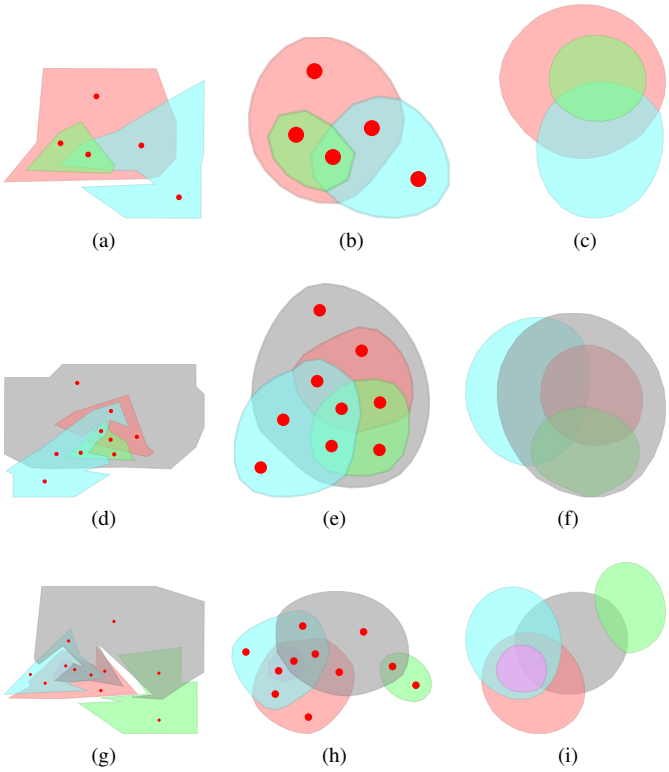

Fig. 12: Comparison of diagrams optimised with `EulerSmooth` and with `EulerForce`. In order to preserve the zone spacing with `EulerSmooth`, a dummy node have been inserted in each depicted zone. First row, example diagram with three sets (instance ID 1). Second row, example diagram with four sets (instance ID 1). Third row, example diagram with five sets (instance ID 2). (a,d,g) The initial diagrams (reconstructed from the `EulerForce` software). (b,e,h) The diagrams optimised with `EulerSmooth` (`Mov`,`Dep`,`Sep`). (c,f,i) The diagrams optimised with `EulerForce` (reconstructed from the `EulerForce` software).

Running times are averaged over five executions and are in the range of one to a dozen of seconds. Times of this magnitude are acceptable for an interactive environment, as long as the data is only updated every few seconds. As expected, larger diagrams and independent with boundaries are generally responsible for increased computation times. However, relatively simple diagrams might still require a relatively high number of iterations. When observing the smoothing over time, we notice that boundary shapes are rapidly smoothed, but that a large amount of time is used to shrink the contours to snugly fit the set elements. In fact, the shrinking process is slower on regular shapes, which are quickly achieved in small and simple instances.

Comparison with EulerForce We run a more in-depth comparison between `EulerSmooth` and `EulerForce`. The authors of `EulerForce` provide a software that can generate an initial random diagram with 3, 4 or 5 sets that can be improved. We generate five diagrams for each number of sets (a total of 15 diagrams) and optimize them using `EulerSmooth` and `EulerForce`. We compare the resulting average isoperimetric quotient and recorded the average running time over the executions for both algorithms. Table 2 reports this data.

The computed metrics indicate a higher set boundary regularity for `EulerForce`, as suggested by visual inspection. The values are high and about the same for both approaches, indicating that all output diagrams are of high quality. However, `EulerForce` does not always produce a valid diagram. It produces an invalid configuration, with introduced and removed zones, for three out of five instances of the five set data set. The authors explain that the increase in diagram complexity increases probability of obtaining invalid configurations, resulting in a success rate of 61% for five sets. As seen in this paper, we can scale to diagrams of twenty sets.

`EulerSmooth`, due to its simple force system, can generate correct and pleasant diagrams even for the instances not supported `EulerForce` every time (see Figure 14). Also, the running time of `EulerSmooth` is below that of `EulerForce` around four to five sets, indicating that it can scale to larger diagrams.

6 Conclusion

In this paper, we present a simple approach for Euler diagram improvement based on a simplification of curve shortening flow. We translate this method into a force system that can be used to improve the output of any Euler diagram drawing method using polygonal curves and set elements. The approach has been demonstrated on a variety of methods [21, 8, 17, 14] for drawing Euler diagrams and evaluated against competitive approaches.

As future work, it would be interesting to see if we can extend other aspects of curve shortening flow and vector field design to the improvement of Euler diagrams in general. As methods exist that do not use a force system to optimize the input shape, it may be beneficial, in terms of computation time, to use these methods instead of the force system to optimize Euler diagrams.

References

[1] B. Alper, N. H. Riche, G. Ramos, and M. Czerwinski. Design study of linesets, a novel set visualization technique. *IEEE Trans. on Visualization and Computer Graphics (InfoVis '11)*, 17(12):2259–2267, 2011.

[2] B. Alsallakh, W. Aigner, S. Miksch, and H. Hauser. Radial sets: Interactive visual analysis of large overlapping sets. *IEEE Trans. on Visualization and Computer Graphics (InfoVis '13)*, 19(12):2496–2505, 2013.

[3] B. Alsallakh, L. Micallef, W. Aigner, H. Hauser, S. Miksch, and P. Rodgers. Visualizing sets and set-typed data: State-of-the-art and future challenges. In *Proc. of Eurographics Conference on Visualization (EuroVis '14) STAR Reports*, pages 1–21, 2014.

[4] G. D. Bader and C. W. V. Hogue. An automated method for finding molecular complexes in large protein interaction networks. *BMC Bioinformatics*, 4(2):27, 2003.

[5] F. Bertault. A force-directed algorithm that preserves edge crossing properties. *Information Processing Letters*, 74(1–2):7–13, Apr. 2000.

[6] A. Blake, G. Stapleton, P. Rodgers, L. Cheek, and J. Howse. The impact of shape on the perception of euler diagrams. In *Proc. of the 8th International Conference on the Theory and Application of Diagrams*, volume 8578 of *LNAI*, pages 124–138, 2014.

[7] G. Chen, K. Mischaikow, R. S. Laramee, P. Pilarczyk, and E. Zhang. Vector field editing and periodic orbit extraction using morse decomposition. *Visualization and Computer Graphics, IEEE Transactions on*, 13(4):769–785, 2007.

[8] C. Collins, G. Penn, and S. Carpendale. Bubble Sets: Revealing set relations with isocontours over existing visualizations. *IEEE Trans. on Visualization and Computer Graphics (InfoVis '09)*, 15(6):1009–1016, 2009.

[9] M. Desbrun, M. Meyer, P. Schröder, and A. H. Barr. Implicit fairing of irregular meshes using diffusion and curvature flow. In *Proceedings of the 26th annual conference on Computer graphics and interactive techniques*, pages 317–324. ACM Press/Addison-Wesley Publishing Co., 1999.

[10] L. Euler. Lettres à une princesse d'allemagne. *letters no. 102-108*, 1761.

[11] H. A. Kestler, A. Mller, J. M. Kraus, M. Buchholz, T. M. Gress, H. Liu, D. W. Kane, B. R. Zeeberg, and J. N. Weinstein. VennMaster: Area-proportional euler diagrams for functional go analysis of microarrays. *BMC Bioinformatics*, 9(1), 2008.

[12] K. Koffka. *Principles of Gestalt Psychology*. Harcourt Brace, 1935.

[13] L. Micallef and P. Rodgers. eulerAPE: Drawing area-proportional 3-venn diagrams using ellipses. *PLoS One*, 9(7):101717, 2014.

[14] L. Micallef and P. Rodgers. eulerForce: Force-directed layout for euler diagrams. *Journal of Visual Languages and Computing*, 25(6):924–934, 2014.

[15] G. Palla, I. Derényi, I. Farkas, and T. Vicsek. Uncovering the overlapping community structure of complex networks in nature and society. *Nature*, 435:814–818, 2005.

[16] S. E. Palmer. Common region: a new principle of perceptual grouping. *Cognitive Psychology*, 24(3):436–447, 1992.

[17] N. H. Riche and T. Dwyer. Untangling euler diagrams. *IEEE Trans. on Visualization and Computer Graphics (InfoVis '10)*, 16(6):1090–1099, 2010.

[18] P. Rodgers, L. Zhang, and A. Fish. General euler diagram generation. In *Diagrammatic Representation and Inference*, volume 5223 of *LNCS*, pages 13–27. Springer, 2008.

[19] P. Rodgers, L. Zhang, G. Stapleton, and A. Fish. Embedding wellformed euler diagrams. In *Proc. of the 12th International Conference on Information Visualisation*, pages 585–593, 2008.

[20] P. Simonetto, D. Archambault, D. Auber, and R. Bourqui. ImPrEd: An improved force-directed algorithm that prevents nodes from crossing edges. *Computer Graphics Forum (EuroVis '11)*, 30(3):1071–1080, 2011.

[21] P. Simonetto, D. Auber, and D. Archambault. Fully automatic visualisation of overlapping sets. *Computer Graphics Forum (EuroVis '09)*, 28(3):967–974, 2009.

[22] G. Stapleton, J. Flower, P. Rodgers, and J. Howse. Automatically drawing euler diagrams with circles. *Journal of Visual Languages & Computing*, 23(3):163–193, 2012.

[23] G. Stapleton, P. Rodgers, J. Howse, and L. Zhang. Inductively generating euler diagrams. *IEEE Trans. on Visualization and Computer Graphics*, 17(1):88–100, 2011.

[24] G. Taubin. Curve and surface smoothing without shrinkage. In *Proc. of the Fifth International Conference on Computer Vision*, pages 852–857, 1995.

[25] G. Taubin. A signal processing approach to fair surface design. In *Proceedings of the 22nd annual conference on Computer graphics and interactive techniques*, pages 351–358. ACM, 1995.

[26] A. Treisman and J. Souther. Search asymmetry: a diagnostic for preattentive processing of separable features. *Journal of Experimental Psychology: General*, 114(3):285–310, 1985.

[27] A. Verroust and M.-L. Viaud. Ensuring the drawability of extended euler diagrams for up to 8 sets. In *Diagrammatic Representation and Inference*, volume 2980 of *LNCS*, pages 128–141. Springer, 2004.

[28] K. Wade, D. Greene, C. Lee, D. Archambault, and P. Cunningham. Identifying representative textual sources in blog networks. In *Proc. of the International Conference on Weblogs and Social Media (AAAI ICWSM)*, pages 393–400, 2011.

[29] L. Wilkinson. Exact and approximate area-proportional circular venn and euler diagrams. *IEEE Trans. on Visualization and Computer Graphics*, 18(2):321–331, 2012.

[30] D. Wyatt, D. Wynn, and P. Clarkson. Set visualiser, 2009. `https://www-edc.eng.cam.ac.uk/tools/set_visualiser/`.

[31] C.-Y. Yao, M.-T. Chi, T.-Y. Lee, and T. Ju. Region-based line field design using harmonic functions. *Visualization and Computer Graphics, IEEE Transactions on*, 18(6):902–913, 2012.